Electronic Supplementary Information

The redox-coupled proton-channel opening in cytochrome *c* oxidase

Alexander Wolf[a], Jovan Dragelj[b], Juliane Wonneberg[a], Johannes Stellmacher[a], Jens Balke[a], Anna Lena Woelke[b,d], Milan Hodoscek[b,c], Ernst Walter Knapp[b], and Ulrike Alexiev[a,*]

[a] Physics Department, Freie Universität Berlin, 14195 Berlin, Germany
[b] Institute of Chemistry and Biochemistry, Freie Universität Berlin, 14195 Berlin, Germany
[c] National Institute of Chemistry, Hajdrihova 19, SI-1001 Ljubljana, Slovenia
[d] Department of Chemistry, University of Cambridge, Cambridge CB2 1EW, UK

* corresponding author: Ulrike Alexiev: Ulrike.alexiev@fu-berlin.de
phone: +49-30-838 55157

Table of content

Materials and Experimental methods

Oxidation and reduction of CcO

Full oxidation and reduction of the enzyme was achieved by addition of potassium hexacyanido ferrate and sodium dithionite, respectively, and the solution's pH adjusted, if necessary.

Spectroscopic experiments

We performed steady-state UV-Vis absorbance spectroscopic measurements on a Shimadzu UV2450 spectrophotometer against a reference cuvette containing buffer solution. Titration and measurements were carried out in a 1 × 1 cm quartz cuvette at 20 °C. We adjusted the pH with small aliquots of diluted NaOH and HCl in the range from pH 5.5 and 9.0. We generated the pH-titration curves from the respective absorbance values at the bound dye's absorbance maximum. Steady-state fluorescence spectroscopy was performed on a HORIBA Jobin-Yvon Fluoromax-3 fluorescence spectrometer in a 0.3 × 0.3 cm quartz cuvette. Fluorescein excitation was done at 484 nm, BADAN excitation at 390 nm.

For spectral decomposition[1], we fitted the fluorescence emission spectra of C*c*O-ADAN with a linear combination of log-normal functions:

$$I_j(\vartheta) = I_{m,j} \times \exp\left(-\left(\frac{\ln 2}{\ln^2 \rho_j}\right) \times \ln^2\left(\frac{a_j - \vartheta}{a_j - \vartheta_{m,j}}\right)\right), \qquad \vartheta < a_j$$
$$I_j(\vartheta) = 0, \qquad \vartheta \geq a_j \tag{1}$$

where $I_{m,j}$ is the peak intensity of fluorescence species j, $\vartheta_{m,j}$ is its maximum intensity wavenumber, a_j is a function limiting point, $\rho_j = \left(\vartheta_{m,j} - \vartheta_{-,j}\right)/\left(\vartheta_{+,j} - \vartheta_{m,j}\right)$ is the band asymmetry parameter with the wavenumber positions of the left and right half maximal amplitudes $\vartheta_{-,j}$, and $\vartheta_{+,j}$.

Titration and pK determination

pH-titrations were performed in 2 mM potassium phosphate buffer solution, 100 mM sodium chloride, 0.05 % β-dodecyl-maltoside. Determination of the respective pK_a values was achieved by fitting the 498 nm fluorescein absorbance with the Henderson-Hasselbalch equation:

$$A = B \times (10^{-\mathrm{p}K_\mathrm{a}}/(10^{-\mathrm{p}K_\mathrm{a}} + 10^{-\mathrm{pH}})) + A_0 \ , \tag{2}$$

where *B* and A_0 are the differences in 498 nm extinction between the dianionic and monoanionic forms of acetamido-fluorescein and residual absorbance from the dye and C*c*O, respectively. The curves where then normalized using *B* and A_0 to compare them to the MD data.

Time-resolved fluorescence spectroscopy

Time-resolved fluorescence polarization decay measurements were conducted with a tunable picosecond Titan-Sapphire laser at 484 nm linearly polarized excitation (240 µW, 4 MHz) in a time correlated single photon counting (TCSPC) setup.[2-4] Emission was passed through a 515 nm long pass filter (OG515), a polarizer alternatingly set to 0° and 90°C for parallel and perpendicular polarization with regard to the excitation light and measured with a microchannel plate detector[5]. Fluorescence decay traces were collected in 1024 time channels with a channel width of 19.7 ps. The instrumental response function (IRF) of the time-correlated single photon counting setup was determined at the corresponding wavelengths with a colloidal silica solution as scattering material (LUDOX, Grace). The instrumental response function of the system had a full width at half-maximum of 30–40 ps.

For time-dependent fluorescence shift (TDFS) measurements a white-light laser source (Supercontinuum, NKT Photonics, Denmark) was used. Furthermore, the detector was changed to a spectrally resolved MW-FLIM detector (Becker & Hickl, Germany) and time-resolved fluorescence measurements were performed with excitation at 405 nm and emission between 422.1 nm and 612.3 nm.

The C*c*O sample buffer was 20 mM potassium phosphate buffer solution at pH 8.0, 20 mM sodium chloride, 0.05 % β-dodecyl-maltoside.

Data analysis was performed with the program GLOBALS Unlimited with data deconvolution with the instrumental response function and fitting of the fluorescence decay traces with a sum of exponentials. [3] The anisotropy is calculated in GLOBALS Unlimited from the intensities *I* measured with parallel and perpendicular polarizer orientation according to

$$r(t) = I_{\parallel}(t) - I_{\perp}(t) / \left(I_{\parallel}(t) + 2I_{\perp}(t) \right) \quad . \tag{3}$$

The anisotropy data is then fitted according to

$$r(t) = r_0 \ \sum_i \beta_i^* \, e^{-t/\varphi_i} + \ r_\infty \quad , \tag{4}$$

where r_0 and r_∞ are the initial and final anisotropy values and β^*_i and φ_i the respective relative amplitudes and decay times for the different anisotropy components. In general, the first component is said to belong to the fluorescent label itself, the second to the loop the dye is attached to, and the third component to the motion of the entire protein itself.[3] The half-cone angle ϑ_M related to the restricted motion of the dye in the commonly employed wobbling-in-a-cone model[6] is related to initial and final anisotropy according to

$$A_\infty = r_\infty / r_0 = \left(\frac{1}{2}\cos\theta_M\,(1+\cos\theta_M)\right)^2 \quad . \tag{5}$$

The more complex cone-in-a-cone model[6] dye and protein motion are assumed to be uncoupled resulting in a multicomponent anisotropy decay:

$$r(t) = r_0\left((1-A_1)e^{-t/\varphi_1}+A_1\right)\left((1-A_2)e^{-t/\varphi_2}+A_2\right)e^{-t/\varphi_G} \quad , \tag{6}$$

where the indices represent the individual parameters for the dye and loop motion and φ_G is the characteristic time for the motion of the entire protein. Two different half-cone angles can be deduced from the two amplitudes A_1 and A_2 in analogy to equation (5).

For TDFS, we determined the emission maximum over time from the fluorescence decays of oxidized and reduced K299C-ADAN mutants in 20 mM potassium phosphate buffer solution at pH 8.0, 20 mM sodium chloride, 0.05 % β-dodecyl-maltoside. Excitation of the samples was performed with a white-light laser source (SuperKExtreme EUV3, NKT Photonics) adjusted to 405 nm, a confocal scanning unit (DCS120, Becker&Hickl), and measured with a spectrally resolved 16-channel Gallium arsenide phosphide MW-FLIM detector (PML-16-GASP, Becker&Hickl) in the range (422.1-612.3) nm and TCPSC electronics (SPC150, Becker&Hickl) in a confocal setup. Picosecond fluorescence decays were subsequently extracted and IRF deconvolution performed with a self-written software. Due to the operating characteristics of the spectrally resolved detector allowing for the detection of fluorescence within 16 discrete wavelength bands (widths ~12nm each), emission peaks were approximated with a Gaussian in the high intensity range to determine the maxima with nanometer accuracy. The time-zero emission maximum $\nu(0)$ was determined according to published procedures[7] from the absorbance and emission of the dye in cyclohexane and the absorbance of the protein-dye conjugate in buffer solution. As the absorbance of dithionite, which is needed for C*c*O reduction, interfered with the absorbance of C*c*O-ADAN below 400 nm, the same absorbance was assumed for the reduced enzyme as measured for the oxidized construct. The solvent relaxation correlation was then calculated according to

$$C(t) = \frac{\nu(t)-\nu(\infty)}{\nu(0)-\nu(\infty)} \quad , \tag{7}$$

with $\nu(\infty)$ being the final emission wavenumber estimated from a monoexponential fit of the measured TDFS data points. The solvent relaxation times τ_{SR} could then be determined with the integral over the biexponential fit of the solvent relaxation correlation

$$\tau_{SR} = \int_0^\infty C(t)\,\mathrm{d}t \quad . \tag{8}$$

Computational Methods

Modeling and MD simulations. Modeling and molecular dynamics (MD) simulations of the C*c*O protein membrane complex was performed with the CHARMM22 force field [8], the CHARMM36 extension for lipids [9] and in-house determined parameters for the cofactors[10] and fluorescein (Flu) (see below). Similar computations of C*c*O were performed previously.[10-15] Coordinates of C*c*O for the subunits 1 and 2 from *P. denitrificans* were obtained from the Protein Data Bank [16] (PDB code: 3HB3[17, 18]). The Flu coordinates were taken from the crystal structure of carbonic anhydrase II (PDB code: 2F14[19]) involving Flu as inhibitor. C*c*O was placed in a modeled lipid bilayer of phosphatidylcholines using the plug-in of VMD[20] and embedded in a TIP3P[21] water box with periodic boundary conditions. The carboxylic group of Flu was kept deprotonated, while one of the two oxygens at the triple aromatic ring system can be protonated. In the MD simulations and electrostatic energy computations both oxygens were considered deprotonated or either one of these oxygens was protonated.

MD simulations of up to 47 ns were performed for the O and R state of C*c*O using NAMD[22]. Allowing for detailed equilibration only the last 30 ns were used for analysis. (In the fully oxidized O state the BNC given as heme-a_3(Fe^{III}-$OH^{\bullet}$)/Cu_B^{II}-H_2O/Tyr280-$O^{\bullet}$ and heme-*a* and Cu_A are oxidized. In the reduced state, the composition of BNC is heme-a_3(Fe^{II}-H_2O)/Cu_B^{I}-H_2O/Tyr280-OH and heme-*a* and Cu_A are reduced.) With preliminary MD simulations an optimal orientation of the triple ring of Flu was chosen.

Atomic partial charges of fluorescein

The charges of fluorescein were calculated with a protocol used in previous work[10] and earlier applications[23] with the quantum chemical (QC) program Jaguar v.7.7 using DFT with the B3LYP functional and 6-31g** basis set.[24] First the geometry of fluorescein was optimized quantum chemically. Thereby hydrogen atoms were optimized without any constraints, while other atoms were optimized with respect to bond lengths and bond angles, keeping the corresponding torsion angles fixed at the conformation from a crystal structure of fluorescein (PDB code: 2F14[19]). Next, the electrostatic potential around fluorescein was computed based on the electronic wave function and nuclear charges employing the same QC procedure as in case of geometry optimization. The atomic partial charges were determined based on these electrostatic potentials, by using a two-stage restraint-electrostatic-potential (RESP)[25, 26] procedure. The atomic partial charges of fluorescein are listed in Figure S6.

Computations of pK_A values. The electrostatic energy terms necessary for the evaluation of pK_A values were determined by solving the linearized Poisson-Boltzmann (LPB) equation numerically with APBS [27]. A three-fold grid focusing procedure was used to obtain sufficiently precise results using a spacing of 0.3 Å for the finest grid. [27, 28] The protein and membrane volume was filled with dielectric continuum of dielectric constant $\varepsilon = 4$. Outside the dielectric constant was set to $\varepsilon = 80$ corresponding to water. Implicit ion concentration of 100 mM was used. The protonation pattern of the C*c*O crystal structure at pH 7.0 was evaluated with vanishing atomic partial charges of the

membrane moiety and fixed for all MD simulations, except for Flu and two histidines (His73^{B} and His526^{A}) that are close to Flu. However, explicit atomic charges in the membrane were used for evaluating fluorescein pK_A values from MD simulation time frames. Based on these MD simulations the two histidines are protonated.

Computation of fluorescence depolarization. The time-dependence of fluorescence depolarization were evaluated with

$$r(t) = \frac{2}{5} \langle P_2\big(\vec{\mu}_a(\tau) \cdot \vec{\mu}_b(\tau + t)\big)\rangle_\tau \quad , \tag{9}$$

where P_2 is the second order Legendre polynomial, $\vec{\mu}_a$ and $\vec{\mu}_b$ are the unit length transition dipole vectors for absorption and emission spectroscopy and $\langle\ \rangle_\tau$ denotes the temporal average. These vectors are assumed to be along the length axis of the triple aromatic ring system of Flu. The triangular brackets denote the ensemble average, which in the computation is replaced by a time average. Since the time available for averaging shrinks with the time increment t, the computed decay function $r(t)$ is only displayed for the first few nanoseconds.

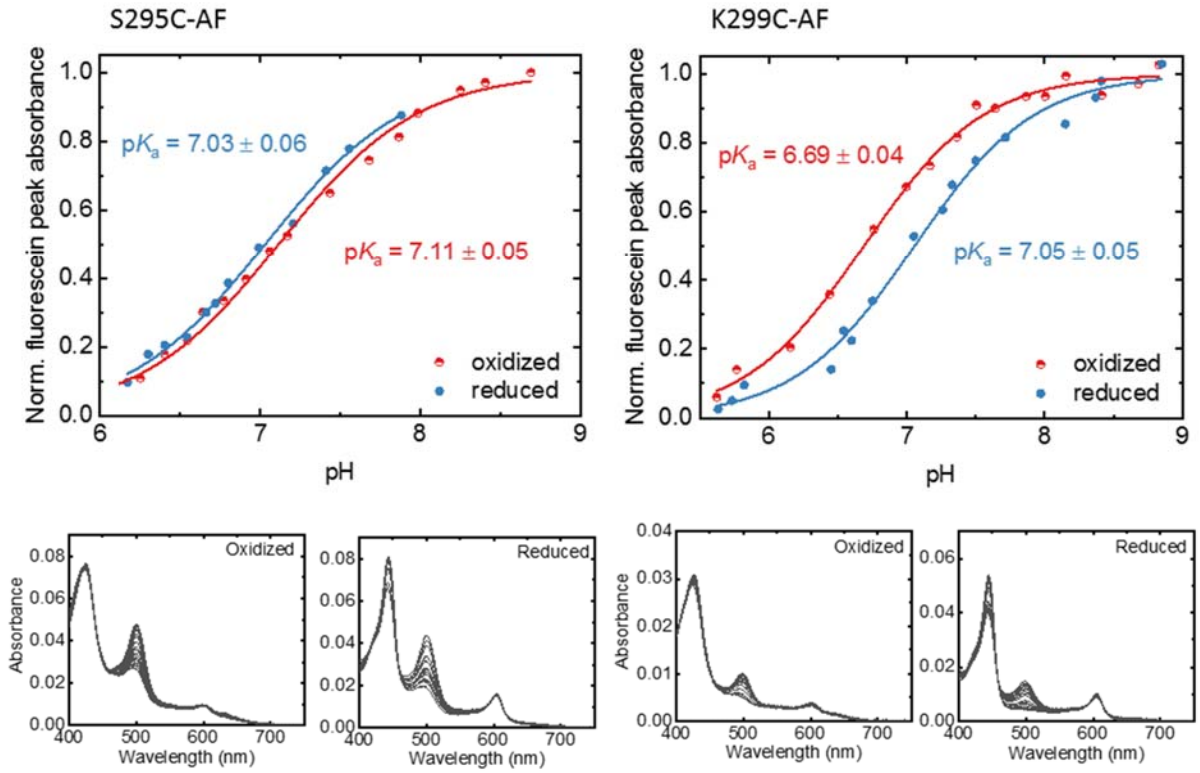

Figure S1: pH-titrations of S295C-AF and K299C-AF.

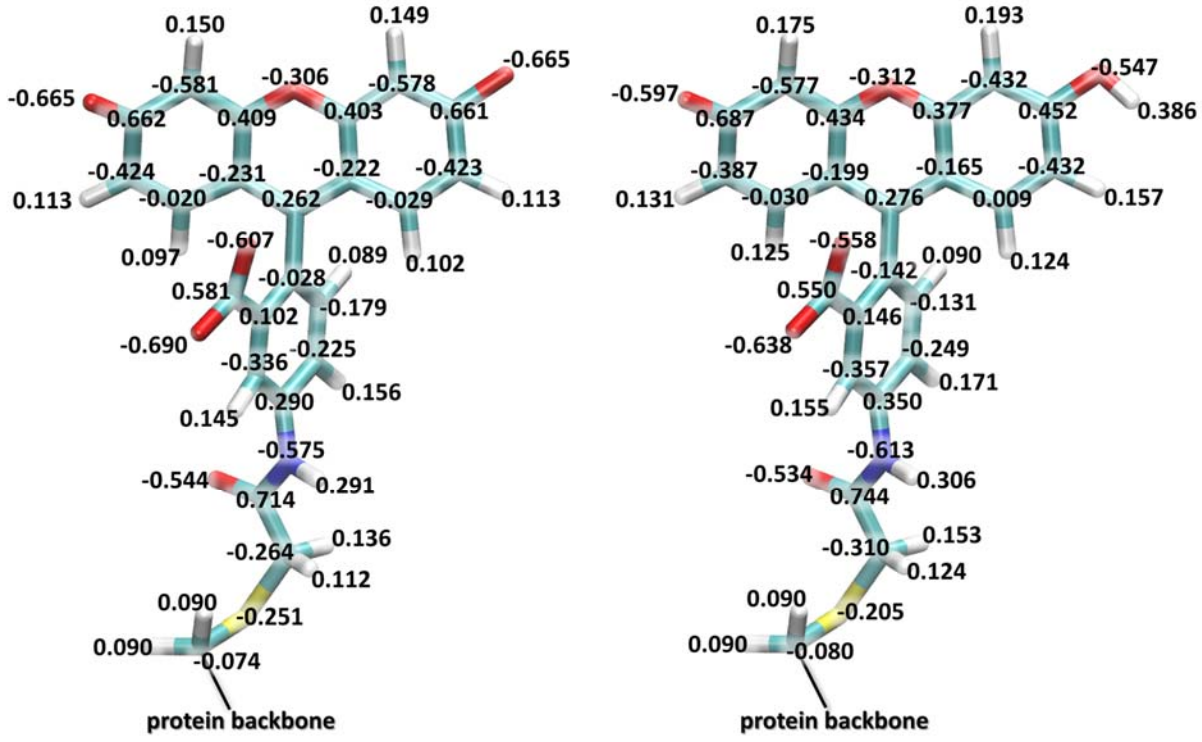

Figure S2. Atomic partial charges of deprotonated (left) and protonated (right) fluorescein and the linker from quantum chemical computations as described above.

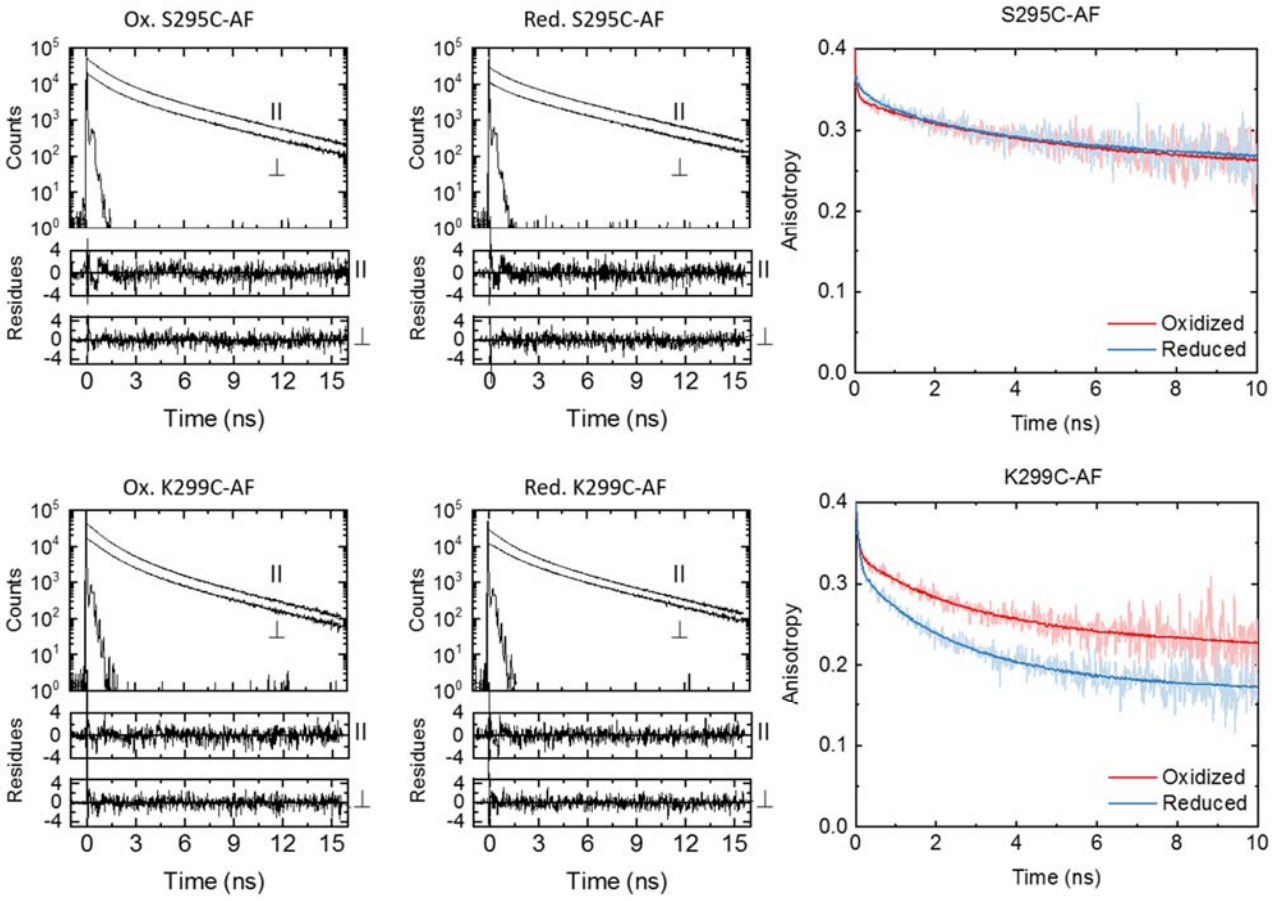

Figure S3: Time-resolved anisotropy data of CcO-K299C-AF and CcO-S295C-AF in the oxidized and reduced state of the enzyme. The goodness of the fit is judged by the residuals and the reduced χ^2. The fit data are summarized in Table S1.

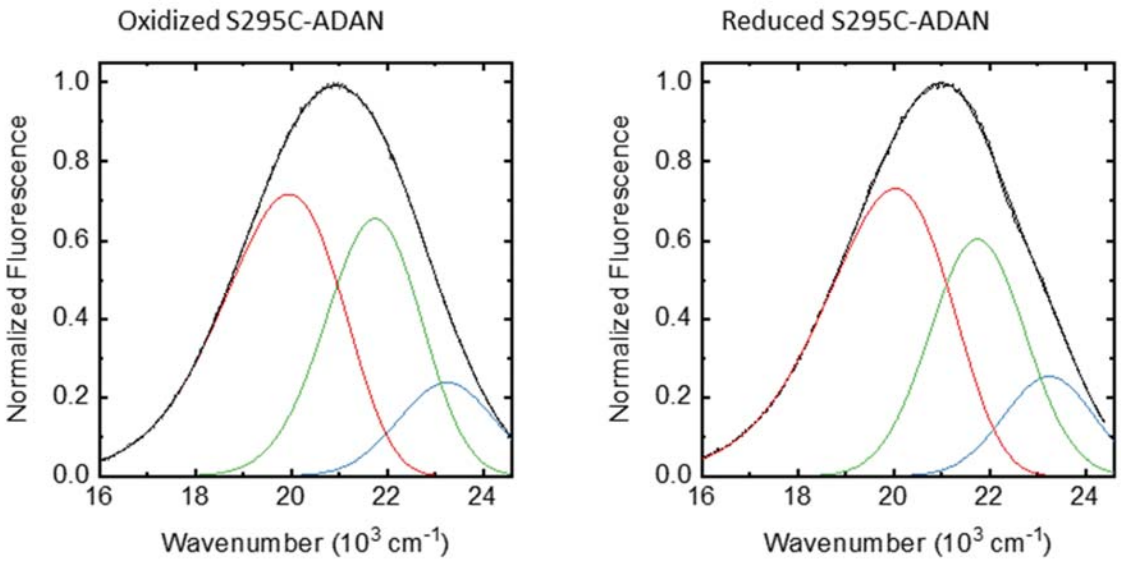

Figure S4: Log-normal spectral decomposition of S295C-ADAN emission spectra. Colors denote the different spectral species: ICT in blue, $HICT_i$ in green, and $HICT_m$ in red.

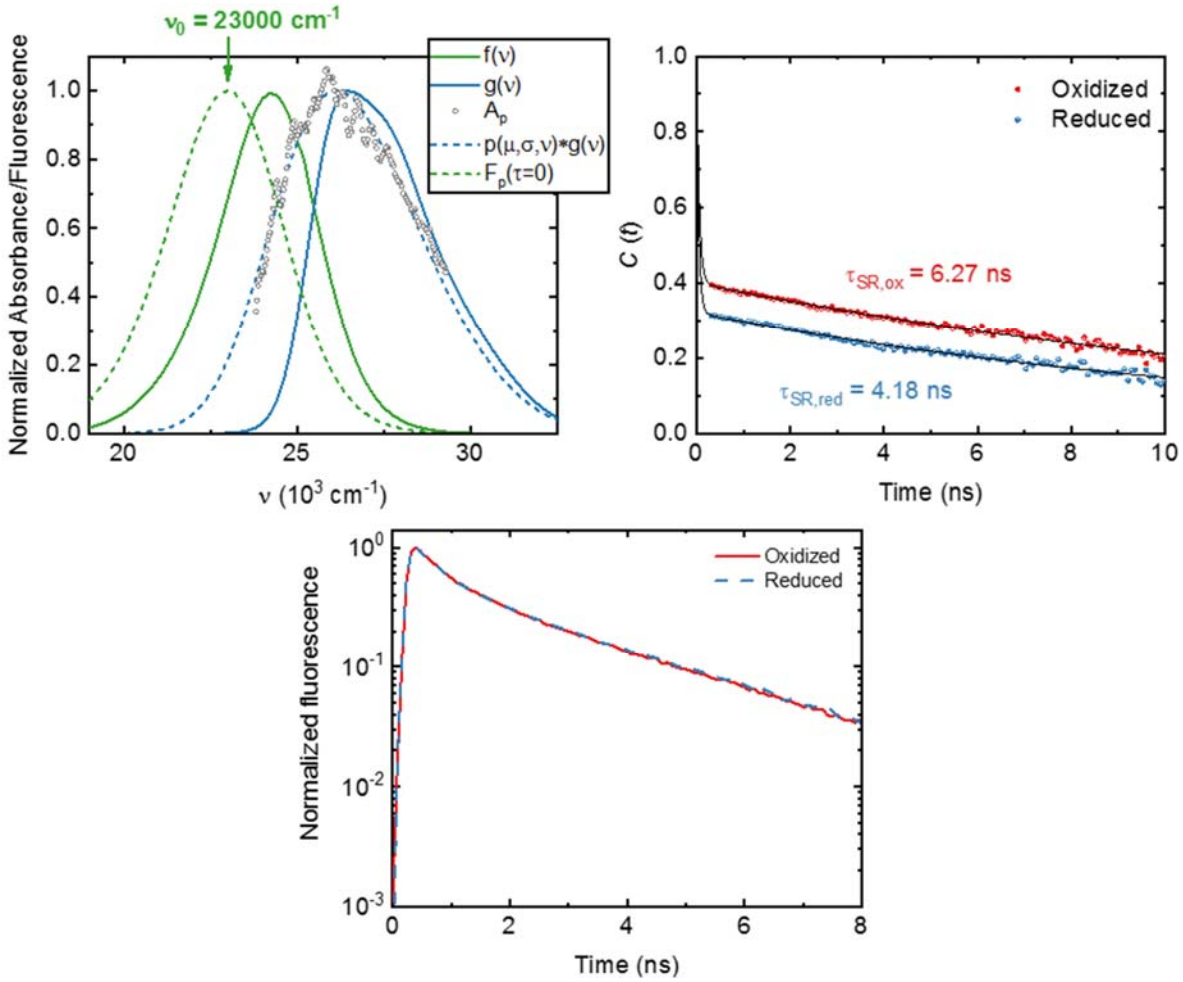

Figure S5: Top left: Determination of K299C-ADAN time-zero emission spectrum and the spectra used for its calculation. Blue full line: nonpolar absorbance line shape function g(*v*). Green full line: nonpolar emission line shape function f(*v*). Circles: BADAN absorbance A_p from C*c*O-K299C-ADAN in H_20. Dashed blue line: Fit of this absorbance with the convolution p*g that includes the inhomogeneous broadening. Dashed green line: Calculated time-zero emission F_p of C*c*O-CS-K299C-ADAN in H_2O at 405 nm excitation with emission maximum at 23000 cm^{-1}. Top right: Autocorrelation with characteristic solvent relaxation times. Monoexponential fits are the black lines (see experimental methods). Red: oxidized enzyme, Blue: reduced enzyme. Bottom: Normalized fluorescence decay curves for both oxidized and reduced CcO-CS-K299C-ADAN at 474 nm emission (bandwidth $\pm$ 6.25 nm).

Table S1: Time-resolved anisotropy fit data. r_0 is the initial anisotropy, β_i^* are the relative amplitudes of the decay components *i* with their characteristic times φ_i, Θ_M is the maximal half-cone angle, and χ^2_{red} gives the quality of the fit.

Sample	State	r_0	β_1^*	β_2^*	β_3^*	φ_1 (ns)	φ_2 (ns)	φ_3 (ns)	Θ_M (°)	χ^2_{red}
S295C-AF	Oxidized	0.359	0.071	0.173	0.768	0.082	3.42	135	23.8	1.18
	Reduced	0.360	0.056	0.168	0.786	0.248	2.62	135	22.7	1.21
K299C-AF	Oxidized	0.367	0.108	0.277	0.645	0.092	2.67	135	30.4	1.19
	Reduced	0.378	0.182	0.421	0.474	0.097	2.42	135	39.2	1.04

Table S2: Fit values from spectral decomposition of emission spectra of BADAN bound to S295C and K299C. $A_{rel,j}$ is the relative amplitude of a species *j* with emission maximum $\nu_{m,j}$.

Sample	State	$A_{rel,1}$ (%)	$\nu_{m,1}$ (10^3 cm^{-1})	$A_{rel,2}$ (%)	$\nu_{m,2}$ (10^3 cm^{-1})	$A_{rel,3}$ (%)	$\nu_{m,3}$ (10^3 cm^{-1})
S295C-ADAN	Oxidized	12.91	23.246	36.25	21.749	50.84	19.952
	Reduced	13.04	23.246	33.03	21.749	53.93	20.036
K299C-ADAN	Oxidized	4.86	23.251	39.78	21.958	55.35	20.085
	Reduced	7.68	23.251	22.19	21.958	70.13	20.306

References

1. E. A. Burstein and V. I. Emelyanenko, *Photochem. Photobiol.*, 1996, **64**, 316-320.
2. T. Y. Kim, M. Moeller, K. Winkler, K. Kirchberg and U. Alexiev, *Photochem. Photobiol.*, 2009, **85**, 570-577.
3. U. Alexiev, I. Rimke and T. Pohlmann, *J. Mol. Biol.*, 2003, **328**, 705-719.
4. K. Kirchberg, T. Y. Kim, M. Möller, D. Skegro, G. D. Raju, J. Granzin, G. Buldt, R. Schlesinger and U. Alexiev, *P Natl Acad Sci USA*, 2011, **108**, 18690-18695.
5. T. Y. Kim, K. Winkler and U. Alexiev, *Photochem. Photobiol.*, 2007, **83**, 378-384.
6. G. F. Schröder, U. Alexiev and H. Grubmuller, *Biophys. J.*, 2005, **89**, 3757-3770.
7. P. Jurkiewicz, J. Sykora, A. Olzynska, J. Humplickova and M. Hof, *J. Fluoresc.*, 2005, **15**, 883-894.
8. B. R. Brooks, C. L. Brooks, A. D. Mackerell, L. Nilsson, R. J. Petrella, B. Roux, Y. Won, G. Archontis, C. Bartels, S. Boresch, A. Caflisch, L. Caves, Q. Cui, A. R. Dinner, M. Feig, S. Fischer, J. Gao, M. Hodoscek, W. Im, K. Kuczera, T. Lazaridis, J. Ma, V. Ovchinnikov, E. Paci, R. W. Pastor, C. B. Post, J. Z. Pu, M. Schaefer, B. Tidor, R. M. Venable, H. L. Woodcock, X. Wu, W. Yang, D. M. York and M. Karplus, *J. Comput. Chem.*, 2009, **30**, 1545-1614.
9. F. J. A. Klauda Jb Venable Rm and et al., *Biophys. J.*, 2010, **72**, 2002-2013.
10. A. L. Woelke, G. Galstyan, A. Galstyan, T. Meyer, J. Heberle and E.-w. Knapp, *J. Phys. Chem. B*, 2013, **117**, 12432-12441.
11. A. L. Woelke, G. Galstyan and E. W. Knapp, *Biochim. Biophys. Acta, Bioenerg.*, 2014, **1837**, 1998-2003.
12. A. L. Woelke, A. Wagner, G. Galstyan, T. Meyer and E. W. Knapp, *Biophys. J.*, 2014, **107**, 2177-2184.
13. D. M. Popovic and A. A. Stuchebrukhov, *J. Am. Chem. Soc.*, 2004, **126**, 1858-1871.
14. V. R. Kaila, M. I. Verkhovsky and M. Wikström, *Chem. Rev.*, 2010, **110**, 7062-7081.
15. P. Goyal, J. Lu, S. Yang, M. R. Gunner and Q. Cui, *P Natl Acad Sci USA*, 2013, **110**, 18886-18891.
16. H. M. Berman, *Nucleic Acids Res.*, 2000, **28**, 235-242.
17. C. Ostermeier, A. Harrenga, U. Ermler and H. Michel, *P Natl Acad Sci USA*, 1997, **94**, 10547-10553.
18. J. Koepke, E. Olkhova, H. Angerer, H. Muller, G. Peng and H. Michel, *Biochim. Biophys. Acta*, 2009, **1787**, 635-645.
19. V. Alterio, R. M. Vitale, S. M. Monti, C. Pedone, A. Scozzafava, A. Cecchi, G. De Simone and C. T. Supuran, *J. Am. Chem. Soc.*, 2006, **128**, 8329-8335.
20. W. Humphrey, A. Dalke and K. Schulten, *J. Mol. Graphics*, 1996, **14**, 33-38.
21. W. L. Jorgensen, J. Chandrasekhar, J. D. Madura, R. W. Impey and M. L. Klein, *J. Chem. Phys.*, 1983, **79**, 926-926.
22. J. C. Phillips, R. Braun, W. Wang, J. Gumbart, E. Tajkhorshid, E. Villa, C. Chipot, R. D. Skeel, L. Kal and K. Schulten, *J. Comput. Chem.*, 2005, **26**, 1781-1802.
23. H. Ishikita and E. W. Knapp, *J. Biol. Chem.*, 2003, DOI: 10.1074/jbc.M306434200.
24. L. L. C. Schrödinger, 2010, LLC, New York, NY-LLC, New York, NY.
25. C. C. I. Bayly, P. Cieplak, W. D. Cornell and P. a. Kollman, *J. Phys. Chem. B*, 1993, **97**, 10269-10280.
26. W. D. Cornell, P. Cieplak, C. I. Bayly and P. a. Kollman, *J. Am. Chem. Soc.*, 1993, **115**, 9620-9631.
27. N. A. Baker, D. Sept, S. Joseph, M. J. Holst and J. A. McCammon, *P Natl Acad Sci USA*, 2001, **98**, 10037-10041.
28. T. Meyer and E. W. Knapp, *J Chem Theory Comput*, 2015, **11**, 2827-2840.